

**Numerical and exact kinetic energy operator using Eckart conditions with one or several reference geometries: Application to HONO**

David Lauvergnat, Josep M. Luis, Bernard Kirtman, Heribert Reis, and André Nauts

Citation: *The Journal of Chemical Physics* **144**, 084116 (2016); doi: 10.1063/1.4942172

View online: <http://dx.doi.org/10.1063/1.4942172>

View Table of Contents: <http://scitation.aip.org/content/aip/journal/jcp/144/8?ver=pdfcov>

Published by the **AIP Publishing**

---

**Articles you may be interested in**

[Aspects of the Eckart frame ro-vibrational kinetic energy operator](#)

*J. Chem. Phys.* **143**, 064104 (2015); 10.1063/1.4928433

[Rovibrational spectroscopy using a kinetic energy operator in Eckart frame and the multi-configuration time-dependent Hartree \(MCTDH\) approach](#)

*J. Chem. Phys.* **141**, 114101 (2014); 10.1063/1.4895557

[An Eckart-frame kinetic energy operator for tetra-atomic planar molecules](#)

*J. Chem. Phys.* **118**, 7208 (2003); 10.1063/1.1562625

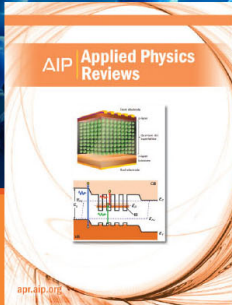
[Exact numerical computation of a kinetic energy operator in curvilinear coordinates](#)

*J. Chem. Phys.* **116**, 8560 (2002); 10.1063/1.1469019

[The triatomic Eckart-frame kinetic energy operator in bond coordinates](#)

*J. Chem. Phys.* **107**, 9493 (1997); 10.1063/1.475291

---



**NEW Special Topic Sections**

**NOW ONLINE**  
Lithium Niobate Properties and Applications:  
Reviews of Emerging Trends

**AIP** | Applied Physics  
Reviews

# Numerical and exact kinetic energy operator using Eckart conditions with one or several reference geometries: Application to HONO

David Lauvergnat,<sup>1,a)</sup> Josep M. Luis,<sup>2</sup> Bernard Kirtman,<sup>3</sup> Heribert Reis,<sup>4,b)</sup> and André Nauts<sup>1,5</sup>

<sup>1</sup>Laboratoire de Chimie Physique, Bâtiment 349, CNRS, UMR8000, Orsay F-91405, France and University of Paris-Sud, Orsay F-91405, France

<sup>2</sup>Institut de Química Computacional and Departament de Química, Universitat de Girona, Campus Montilivi, 17071 Girona, Catalonia, Spain

<sup>3</sup>Department of Chemistry and Biochemistry, University of California, Santa Barbara, California 93106, USA

<sup>4</sup>Department of Chemistry, Faculty of Natural Sciences, Matej Bel University, Tajovského 40, 97400 Banská Bystrica, Slovakia

<sup>5</sup>Institute of Condensed Matter and Nanosciences (NAPS), Université Catholique de Louvain, 2 Chemin du Cyclotron, bte L7.01.07, B-1348 Louvain-la-Neuve, Belgium

(Received 21 July 2015; accepted 4 February 2016; published online 26 February 2016)

For the computation of rovibrational levels and their spectroscopic intensities, the Eckart conditions are essential to achieve the optimal separation between rotation and vibration. Dymarsky and Kudin [J. Chem. Phys. **122**, 124103 (2005)] proposed a procedure for a simplified calculation of the Eckart rotation matrix. In the present work, we have adapted their approach to obtain a kinetic energy operator in curvilinear coordinates using a numerical but exact procedure without resorting to finite differences. Furthermore, we have modified this approach for the study of molecular systems with several minima, for which several Eckart reference geometries are required. The HONO molecular system has been used to show the efficiency of our implementation. Using the Eckart conditions with multi-reference geometries allows for a calculation of the rotational levels as well as frequencies and intensities of the infrared spectra of both HONO isomers with a *single* calculation. © 2016 AIP Publishing LLC. [<http://dx.doi.org/10.1063/1.4942172>]

## I. INTRODUCTION

The rotational Eckart conditions<sup>1</sup> are critical for the calculation of rovibrational spectra. These conditions reduce the Coriolis coupling so that such calculations are less expensive in terms of computational resources and time. Furthermore, since they result in an optimal separation between vibrational and rotational motions (see below), it is easy to get accurate vibrational absorption intensities<sup>2-4</sup> and nonlinear optical properties<sup>5</sup> without including the rotational contribution. The Eckart conditions can be used with rectilinear normal modes,<sup>6-8</sup> in particular with the Watson Hamiltonian<sup>9</sup> or with curvilinear coordinates.<sup>10-13</sup> In the first approach, they are included implicitly while in the second they must be implemented explicitly.

We may write the rotational Eckart conditions as

$$\sum_{\lambda=1}^N m_{\lambda} \cdot \vec{X}_{ref,EC}^{\lambda} \times \vec{X}_{EC}^{\lambda}(\mathbf{Q}) = \vec{0},$$

$$\vec{X}_{ref,EC}^{\lambda} = \begin{bmatrix} X_{ref,EC}^{\lambda,x} \\ X_{ref,EC}^{\lambda,y} \\ X_{ref,EC}^{\lambda,z} \end{bmatrix}, \text{ and } \vec{X}_{EC}^{\lambda}(\mathbf{Q}) = \begin{bmatrix} X_{EC}^{\lambda,x}(\mathbf{Q}) \\ X_{EC}^{\lambda,y}(\mathbf{Q}) \\ X_{EC}^{\lambda,z}(\mathbf{Q}) \end{bmatrix}, \quad (1)$$

where  $N$  is the number of atoms,  $m_{\lambda}$  is the mass of atom  $\lambda$ ,  $\vec{X}_{ref,EC}^{\lambda}$  and  $\vec{X}_{EC}^{\lambda}(\mathbf{Q})$  are the Cartesian coordinates in the Eckart frame ( $EC$ ), the *ref* subscript stands for the reference geometry, and  $\mathbf{Q}$  is the set of  $n$  ( $n \leq 3N - 6$ ) internal deformation coordinates. Several authors<sup>14,15</sup> have shown that these conditions are equivalent to finding the optimal orientation to match the mass-weighted instantaneous geometry and the reference geometry. In other words, the norm (or squared norm) of the mass-weighted squared differences between the Cartesian coordinates of the reference geometry,  $\vec{X}_{ref,EC}^{\lambda}$ , and the displaced one,  $\vec{X}_{EC}^{\lambda}(\mathbf{Q})$ , (Eq. (2)) is minimal for a given  $\mathbf{Q}$ ,

$$\text{Norm}^2 = \sum_{\lambda=1}^N m_{\lambda} \cdot \left\| \vec{X}_{ref,EC}^{\lambda} - \vec{X}_{EC}^{\lambda}(\mathbf{Q}) \right\|^2. \quad (2)$$

The numerical procedure used to apply the Eckart conditions is well known<sup>1,12,16-20</sup> and it is easy to transform Cartesian coordinates from a non-Eckart frame,  $F$ , into an Eckart frame,

$$\vec{X}_{EC}^{\lambda}(\mathbf{Q}) = \mathbf{R}_{EC}(\mathbf{X}(\mathbf{Q}); \mathbf{X}_{ref,EC}) \cdot \vec{X}_F^{\lambda}(\mathbf{Q}). \quad (3)$$

Here,  $\vec{X}_F^{\lambda}$  are the Cartesian coordinates of atom  $\lambda$  in the non-Eckart frame and  $\mathbf{R}_{EC}(\mathbf{X}(\mathbf{Q}); \mathbf{X}_{ref,EC})$  is the Eckart rotation matrix which depends on the reference geometry,  $\mathbf{X}_{ref,EC} = [\vec{X}_{ref,EC}^1 \dots \vec{X}_{ref,EC}^N]$ , as well as the current Cartesian geometry,  $\mathbf{X}(\mathbf{Q}) = [\vec{X}_F^1(\mathbf{Q}) \dots \vec{X}_F^N(\mathbf{Q})]$ . Figure 1 illustrates this transformation for the HONO molecule. In our approach, the Cartesian reference geometries in the non-Eckart and

<sup>a)</sup>E-mail: David.Lauvergnat@lcp.u-psud.fr

<sup>b)</sup>On leave from Institute of Biology, Medicinal Chemistry and Biotechnology, National Hellenic Research Foundation, 48 Vas. Constantinou Ave., Athens 116 35, Greece.

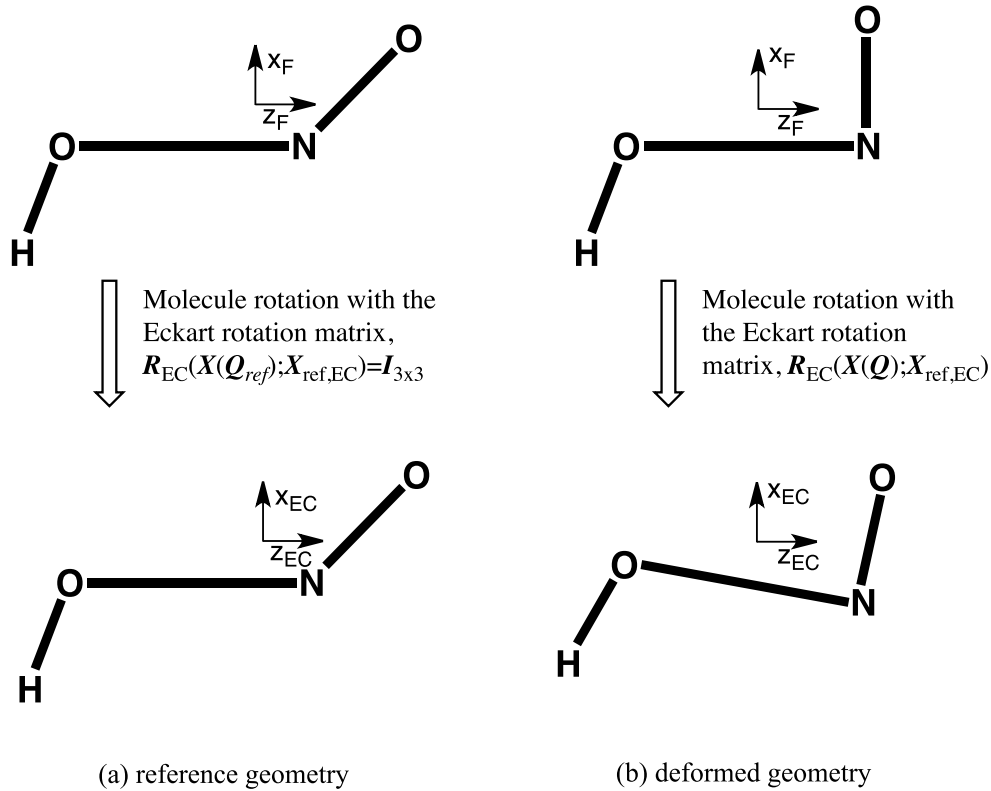


FIG. 1. Illustration of the Eckart rotation matrix for HONO with respect to the non-Eckart frame F and the reference geometry. (a) Reference geometry,  $X_{ref,EC}$ , in the Eckart frame and in the non-Eckart frame are identical. (b) Deformed geometry in the non-Eckart frame (top panel) and deformed geometry in the Eckart frame (bottom panel).

in the Eckart frames are identical, as shown in Fig. 1(a). In other words, the Eckart rotation matrix is the identity matrix (Fig. 1(a)). In the geometry shown in the top panel of Fig. 1(b), the O—N—O angle has been reduced with respect to the reference geometry by moving only the terminal oxygen. The Cartesian coordinates of this deformed geometry are expressed in the non-Eckart frame because it partially contains a counterclockwise rotation of the molecule. The deformed Cartesian geometry has the central ON bond parallel to the z-axis in the non-Eckart frame, while this bond is slightly tilted after the Eckart rotation of the molecule (Fig. 1(b), bottom panel). An illustrative explanation of the Eckart rotation matrix for the water molecule can be found in chapter 10.2 of Ref. 21.

It is worth noting that analytical expressions for the rotational angles are unknown except in the case of small molecules such as triatomics<sup>22,23</sup> or planar molecules.<sup>24,25</sup> Thus, one has to calculate this matrix numerically for a given value of the internal coordinates,  $\mathbf{Q}$ .

If one wants to use Cartesian coordinates in the Eckart frame or to project an operator such as the electric dipole onto this frame, Eq. (3) can be used directly. However, if one wants to develop a kinetic energy operator (KEO) that respects the Eckart conditions, then Eqs. (1) and (3) have to be used with caution. In general, the KEO can be expressed as a sum of three terms,<sup>26</sup> a deformation part,  $\hat{T}_{def}$ , a Coriolis part,  $\hat{T}_{cor}$ , and a rotational part,  $\hat{T}_{rot}$ ,

$$\begin{aligned} \hat{T}_{def} &= -\frac{\hbar^2}{2} \sum_{i,j=1}^n \frac{1}{\rho(\mathbf{Q})} \frac{\partial}{\partial Q^i} \rho(\mathbf{Q}) \Sigma^{ij}(\mathbf{Q}) \frac{\partial}{\partial Q^j} + V_{extra}(\mathbf{Q}) \\ &= -\frac{\hbar^2}{2} \left[ \sum_{i,j} \Sigma^{ij}(\mathbf{Q}) \partial_{ij}^2 + \sum_{i,j} (\partial_i \Sigma^{ij}(\mathbf{Q}) + \Sigma^{ij}(\mathbf{Q}) \partial_i \ln(\rho(\mathbf{Q}))) \partial_j \right] + V_{extra}(\mathbf{Q}), \end{aligned} \quad (4)$$

$$\begin{aligned} \hat{T}_{cor} &= \sum_{\alpha} \hat{J}_{\alpha} \left[ -i\hbar \sum_j \left( \frac{\partial_j \Gamma^{\alpha j}(\mathbf{Q}) + \Gamma^{\alpha j}(\mathbf{Q}) \partial_j \ln(\rho(\mathbf{Q}))}{2} \right) + \Gamma^{\alpha j}(\mathbf{Q}) \partial_j \right] \\ &= \sum_{\alpha} \hat{J}_{\alpha} \hat{T}_{cor}^{\alpha}, \end{aligned} \quad (5)$$

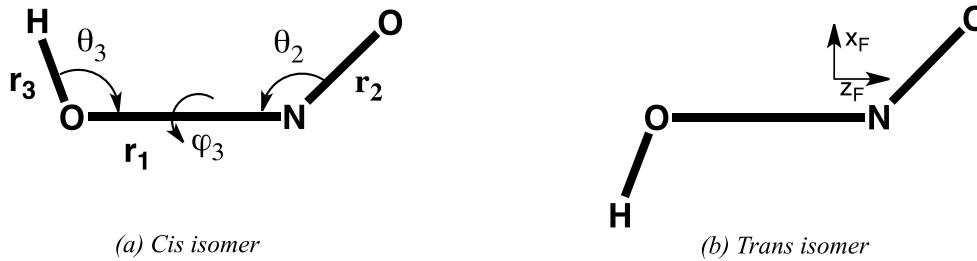


FIG. 2. HONO isomers and orientation of the molecule with respect to the non-Eckart frame, F.

$$\hat{T}_{rot} = \frac{1}{2} \sum_{\alpha, \beta} \mu^{\alpha\beta}(\mathbf{Q}) \hat{J}_\alpha \hat{J}_\beta = \sum_{\alpha, \beta} \hat{T}_{rot}^{\alpha\beta} \hat{J}_\alpha \hat{J}_\beta, \quad (6)$$

$$d\tau_{def} = \rho(\mathbf{Q}) dQ^1 \dots dQ^n, \quad (7)$$

where  $d\tau_{def}$  is the volume element corresponding to the deformation part;  $\rho(\mathbf{Q})$  is a weight function used to normalize the deformation wave functions, which must be adapted to the vibrational basis set; and  $\Sigma^{ij}(\mathbf{Q})$ ,  $\Gamma^{\alpha j}(\mathbf{Q})$ , and  $\mu^{\alpha\beta}(\mathbf{Q})$  are the contravariant components of the metric tensor,  $G^{ij}(\mathbf{Q})$ , which correspond to deformation, Coriolis, and rotational parts, respectively. The term  $V_{extra}(\mathbf{Q})$  appears when a non-Euclidian normalization convention is used and is often called the extra-potential term<sup>26–28</sup> or pseudo-potential term<sup>29</sup> and is given by

$$V_{extra}(\mathbf{Q}) = \frac{\hbar^2}{8} \sum_{i,j}^{n,n} \Sigma^{ij} \left[ \frac{\partial_i \rho}{\rho} \frac{\partial_j \rho}{\rho} - \frac{\partial_i \tilde{J}}{\tilde{J}} \frac{\partial_j \tilde{J}}{\tilde{J}} \right] + \frac{\hbar^2}{4} \sum_{i,j}^{n,n} \left\{ \partial_i \Sigma^{ij} \left[ \frac{\partial_j \rho}{\rho} - \frac{\partial_j \tilde{J}}{\tilde{J}} \right] + \Sigma^{ij} \left[ \frac{\partial_{ij}^2 \rho}{\rho} - \frac{\partial_{ij}^2 \tilde{J}}{\tilde{J}} \right] \right\}, \quad (8)$$

where  $\tilde{J} = \sqrt{\det(\mathbf{g}(\mathbf{Q}))}$  and  $\mathbf{g}(\mathbf{Q})$  is the matrix associated with the covariant components of the metric tensor.

In order to obtain the KEO numerically, as done in TNUM<sup>27</sup> or other programs,<sup>11,28,30–32</sup> derivatives of  $\vec{X}_{EC}^\lambda(\mathbf{Q})$  with respect to  $\mathbf{Q}$  need to be calculated. In the context of the Eckart frame, several approaches have been used. Probably the earliest is due to McCoy *et al.*<sup>16</sup> More recently, a similar approach has been utilized by the Császár group<sup>17,33</sup> and also by Wang and Carrington,<sup>12</sup> who calculate the derivatives by means of finite differences. This requires checking of the convergence with regard to the step size used in the finite difference scheme.

Very recently, Pesonen<sup>34</sup> and Szalay<sup>35</sup> have shown that it is possible to obtain the Eckart frame KEO for curvilinear coordinates without resorting to a finite difference scheme. We will demonstrate herein that it is also possible with TNUM to completely avoid the finite difference scheme and to calculate the derivatives of  $\vec{X}_{EC}^\lambda(\mathbf{Q})$  with respect to  $\mathbf{Q}$  exactly. The exact KEO is evaluated numerically using the Eckart frame and curvilinear coordinates. Furthermore, a small modification of this implementation enables us to derive the Eckart rotation matrix for several reference geometries in a way similar to how the Sayvetz conditions<sup>36</sup> have been employed for

large amplitude motions.<sup>11,37–40</sup> In the latter case, the Eckart reference geometry moves continuously along a one- or multi-dimensional chemical/physical path.

To illustrate our implementation, particularly for the multi-reference Eckart conditions, we use the HONO molecule. This molecule exists in two isomers, the *trans* and the *cis* forms (see Fig. 2), which are separated in energy by only 93 cm<sup>-1</sup>.<sup>41</sup> Richter *et al.*<sup>42</sup> have calculated dipole moment surfaces in a non-Eckart frame, where the z-axis is parallel to the central NO bond and the ONO atoms are in the xz plane (see Fig. 2). The experimental infrared spectrum at room temperature shows transitions for both isomers.<sup>43</sup> Therefore, to calculate the vibrational intensities (Section IV C), we need to apply the Eckart conditions for both isomers or, in other words, we need two Eckart reference geometries, which correspond to the two geometries at the *cis* and *trans* minima.

We will also calculate the rotational levels of both the *cis* and *trans* HONO isomers (Section IV B). It should be noted that the present implementation of the usual Eckart conditions (with a single reference geometry) in TNUM has been used previously in combination with the Multi Configuration Time Dependent Hartree (MCTDH) method to calculate rovibrational levels of H<sub>2</sub>O and HONO.<sup>13</sup> However, the numerical implementation was discussed just briefly and, therefore, more details about this implementation are provided here.

## II. NUMERICAL AND EXACT ECKART KEOs

Before explaining the calculation of the derivatives of  $\vec{X}_{EC}^\lambda(\mathbf{Q})$ , it is important to present briefly the procedure, used in TNUM,<sup>27</sup> to obtain the exact KEO numerically without imposing the Eckart conditions. We<sup>27</sup> are using the so-called  $\mathbf{X}(\mathbf{Q})$  approach, where  $\mathbf{X}$  is the set of body-fixed (BF) Cartesian coordinates. The treatments of McCoy<sup>16</sup> and Carrington,<sup>12</sup> which use the  $\mathbf{Q}(\mathbf{X})$  approach, yield the same KEO. In the group of Császár, the numerical KEO can be obtained by both approaches,<sup>28,44</sup> although they have shown that the  $\mathbf{X}(\mathbf{Q})$  approach is numerically more stable,<sup>23</sup> in particular when a reduced dimensionality treatment is used or when internal coordinates are defined by means of dummy atoms (see also our analysis in Appendix A).

In both the  $\mathbf{X}(\mathbf{Q})$  and  $\mathbf{Q}(\mathbf{X})$  implementations one needs to calculate the contravariant components of the metric tensor,  $G^{ij}(\mathbf{Q})$ . With the  $\mathbf{Q}(\mathbf{X})$  approach, they are calculated directly while in the  $\mathbf{X}(\mathbf{Q})$  approach, the covariant components,  $g_{ij}(\mathbf{Q})$ , are calculated first,

$$G(\mathbf{Q}) = \begin{bmatrix} \boldsymbol{\Sigma}(\mathbf{Q}) & \boldsymbol{\Gamma}'(\mathbf{Q}) \\ \boldsymbol{\Gamma}(\mathbf{Q}) & \boldsymbol{\mu}(\mathbf{Q}) \end{bmatrix} = \mathbf{g}(\mathbf{Q})^{-1} = \begin{bmatrix} \mathbf{S}(\mathbf{Q}) & \mathbf{C}'(\mathbf{Q}) \\ \mathbf{C}(\mathbf{Q}) & \mathbf{I}(\mathbf{Q}) \end{bmatrix}^{-1}. \quad (9)$$

The matrices  $\mathbf{S}$  and  $\mathbf{C}$  are, respectively, the deformation and Coriolis contributions, while  $\mathbf{I}$  is the usual inertia tensor. To calculate the inertia tensor, no derivatives are required. However, the first derivatives of the Cartesian coordinates with respect to internal ones are required to determine  $\mathbf{S}$  and  $\mathbf{C}$ . Indeed, the deformation, Coriolis and inertia parts read

$$S_{ij}(\mathbf{Q}) = \sum_{\lambda=1}^N m_{\lambda} \frac{\partial \vec{X}_F^{\lambda}}{\partial Q^i} \cdot \frac{\partial \vec{X}_F^{\lambda}}{\partial Q^j}, \quad (10)$$

$$C_{\alpha i}(\mathbf{Q}) = \sum_{\lambda=1}^N m_{\lambda} \left[ \vec{X}_F^{\lambda} \times \frac{\partial \vec{X}_F^{\lambda}}{\partial Q^i} \right]^{\alpha}, \quad (11)$$

$$I_{\alpha\beta}(\mathbf{Q}) = \sum_{\lambda=1}^N m_{\lambda} \left( \vec{X}_F^{\lambda} \cdot \vec{X}_F^{\lambda} \delta_{\alpha\beta} - X_F^{\lambda,\alpha} X_F^{\lambda,\beta} \right), \quad (12)$$

where  $\alpha, \beta = [x, y, z]$  and  $[\dots]^{\alpha}$  denotes the  $\alpha$  component of the expression in the square brackets.

In the code TNUM, derivatives (up to third order in  $Q^i$ ), like  $\frac{\partial \vec{X}_F^{\lambda}}{\partial Q^i}$ , are obtained numerically from the exact expressions (see Ref. 27 for more details). In the Eckart context,  $\mathbf{X}(\mathbf{Q})$  needs to be transformed using the Eckart conditions (Eqs. (1) and (3)), i.e.,  $\mathbf{X}(\mathbf{Q})$  must correspond to  $[\vec{X}_{EC}^1, \vec{X}_{EC}^2, \dots, \vec{X}_{EC}^N]$  and, then, the latter is used in Eqs. (4)-(12). The required derivatives, in turn, are calculated

from Eq. (13),

$$\frac{\partial \vec{X}_{EC}^{\lambda}}{\partial Q^i} = \mathbf{R}_{EC}(\mathbf{X}(\mathbf{Q}); \mathbf{X}_{ref,EC}) \cdot \frac{\partial \vec{X}_F^{\lambda}}{\partial Q^i} + \frac{\partial \mathbf{R}_{EC}}{\partial Q^i} \cdot \vec{X}_F^{\lambda}(\mathbf{Q}). \quad (13)$$

It is important to note that when the Eckart conditions are not used,  $\mathbf{X}(\mathbf{Q})$  corresponds to  $[\vec{X}_F^1, \vec{X}_F^2, \dots, \vec{X}_F^N]$ . In previous work, two of us implemented the numerical calculation of  $(\frac{\partial \vec{X}_F^{\lambda}}{\partial Q^i})$  required in Eq. (13) from an exact expression in TNUM.<sup>27</sup> In order to obtain the Eckart rotation matrix  $\mathbf{R}_{EC}$ , and its derivatives,  $\frac{\partial \mathbf{R}_{EC}}{\partial Q^i}$ , in a similar manner, we adapted the approach of Dymarsky and Kudin.<sup>18</sup> In their approach, two  $3 \times 3$  matrices ( $\mathbf{A}_1 = \mathbf{A} \cdot \mathbf{A}^t$  and  $\mathbf{A}_2 = \mathbf{A}^t \cdot \mathbf{A}$ ) are calculated from matrix  $\mathbf{A}$ , with elements and derivatives ( $\alpha, \beta = [x, y, z]$ ) defined by

$$\begin{cases} \mathbf{A}^{\alpha,\beta}(\mathbf{Q}) = \sum_{\lambda=1}^N m_{\lambda} \cdot X_F^{\lambda,\alpha}(\mathbf{Q}) \cdot X_{ref,EC}^{\lambda,\beta} \\ \frac{\partial \mathbf{A}^{\alpha,\beta}(\mathbf{Q})}{\partial Q^i} = \sum_{\lambda=1}^N m_{\lambda} \cdot \frac{\partial X_F^{\lambda,\alpha}(\mathbf{Q})}{\partial Q^i} \cdot X_{ref,EC}^{\lambda,\beta} \end{cases}. \quad (14)$$

As will be seen below, the Eckart rotation matrix is determined from the eigenvectors of  $\mathbf{A}_1$  and  $\mathbf{A}_2$ . By using a modified version of the Jacobi diagonalization procedure, along with the derivatives in Eq. (14), we show in Appendix B how the derivatives of these eigenvectors may be obtained at the same time as the eigenvectors themselves.

The expressions for the Eckart rotation matrix and its derivatives, as given by Dymarsky and Kudin,<sup>18</sup> are

$$\begin{cases} \mathbf{R}_{EC}^{\alpha,\beta} = \sum_{k=1}^3 \mathbf{Vec}_1(k)^{\alpha} \cdot \mathbf{Vec}_2(k)^{\beta} \\ \frac{\partial \mathbf{R}_{EC}^{\alpha,\beta}}{\partial Q^i} = \sum_{k=1}^3 \frac{\partial \mathbf{Vec}_1(k)^{\alpha}}{\partial Q^i} \cdot \mathbf{Vec}_2(k)^{\beta} + \mathbf{Vec}_1(k)^{\alpha} \cdot \frac{\partial \mathbf{Vec}_2(k)^{\beta}}{\partial Q^i} \end{cases}, \quad (15)$$

where  $\mathbf{Vec}_i(k)$  is the  $k$ -th eigenvector of  $\mathbf{A}_i$ . When the deformed geometry is close to the reference geometry, the first and second eigenvectors of  $\mathbf{A}_2$  must be transformed (by multiplying by  $-1$ ) so that the scalar product with the corresponding eigenvectors of  $\mathbf{A}_1$  is positive. Furthermore, the third eigenvector  $\mathbf{Vec}_i(3)$  may be obtained from the vector product  $\mathbf{Vec}_i(1) \times \mathbf{Vec}_i(2)$ . With this robust procedure, we have all the ingredients needed to calculate the Cartesian coordinates,  $\vec{X}_{EC}^{\lambda}(\mathbf{Q})$ , and their derivatives,  $\frac{\partial \vec{X}_{EC}^{\lambda}}{\partial Q^i}$ , in the Eckart frame.

At this point, two comments about what has been presented thus far can be made.

- (i) The determinant of  $\mathbf{R}_{EC}$  has to be unity for all values of the coordinates since it is a rotation matrix. Therefore, its derivative must be zero. This feature has enabled us to check the numerical stability of our implementation.

- (ii) As pointed out by Dymarsky and Kudin,<sup>18</sup> the procedure works well when the deformed geometry,  $\mathbf{X}_{EC}(\mathbf{Q})$ , is close to the reference geometry,  $\mathbf{X}_{ref,EC}$ , or in other words when the Eckart rotation matrix is close to the identity matrix. However, that is not always the case. In particular, it is likely not to be so if one chooses a reference geometry oriented with respect to the principal axes, and it is certainly not the case if the deformed geometry is far away from the Eckart reference geometry (either for a floppy system or when the calculation needs a grid with a large range).

To illustrate what may happen when the deformed geometry is far from the reference geometry, we have used a 1D-model where the internal coordinate is the torsional angle ( $\varphi_3$ ) that describes the *cis-trans* isomerization of HONO. The reference geometry is given by the *trans* configuration.

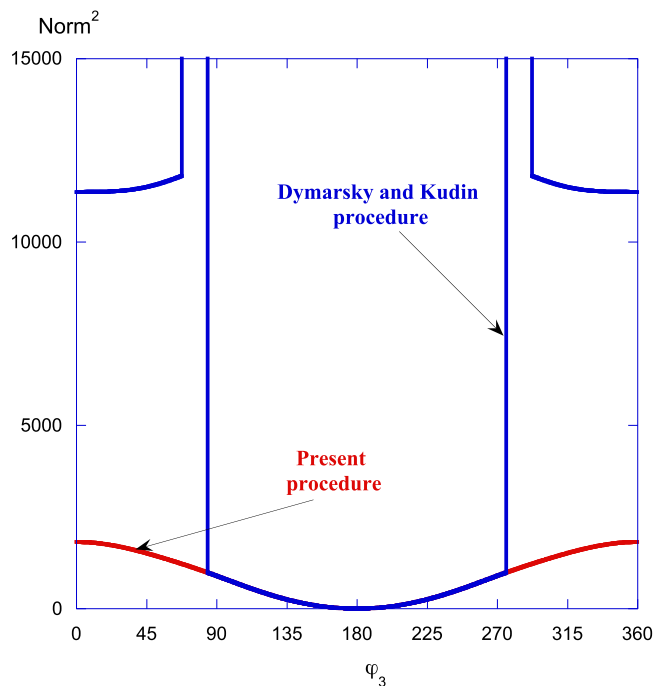


FIG. 3.  $\text{Norm}^2$  (Eq. (2)) as a function of the torsional angle,  $\varphi_3$ , using the Dymarsky and Kudin procedure (blue curve) or our new procedure developed for this work (red curve).

In Fig. 3, the quantity  $\text{Norm}^2$  (Eq. (2)) is plotted as a function of  $\varphi_3$ . The blue curve is obtained when the Dymarsky and Kudin procedure is used, which works very well around the *trans* geometry ( $\varphi_3 = 180^\circ$ ) where  $\text{Norm}^2$  is continuous. However, when the torsional angle is far away from  $180^\circ$  ( $\varphi_3 < 90^\circ$  or  $\varphi_3 > 270^\circ$ ), the value of  $\text{Norm}^2$  increases strongly and becomes discontinuous because the Eckart frame axes flip abruptly. Thus, although the Eckart conditions (Eq. (1)) are satisfied, this approach is not reliable for all regions of the potential energy surface (PES).

Therefore, in our new proposed procedure to avoid the flipping of axes in the Eckart frame, we select the signs of

$$\left\{ \begin{array}{l} A^{\alpha,\beta} = \sum_{\lambda=1}^N m_\lambda \cdot X_F^{\lambda,\alpha}(\mathbf{Q}) \cdot X_{ref,EC}^{\lambda,\beta}(\mathbf{Q}) \\ \frac{\partial A^{\alpha,\beta}}{\partial Q^i} = \sum_{\lambda=1}^N m_\lambda \cdot \frac{\partial X_F^{\lambda,\alpha}(\mathbf{Q})}{\partial Q^i} \cdot X_{ref,EC}^{\lambda,\beta}(\mathbf{Q}) + m_\lambda \cdot X_F^{\lambda,\alpha}(\mathbf{Q}) \cdot \frac{\partial X_{ref,EC}^{\lambda,\beta}(\mathbf{Q})}{\partial Q^i} \end{array} \right. \quad (16)$$

To define the moving Eckart reference geometry, switching functions are employed that smoothly convert one reference geometry into another,

$$\left\{ \begin{array}{l} X_{ref,EC}(\mathbf{Q}) = \sum_{i_{ref}}^{n_{ref}} f_{i_{ref}}(\mathbf{Q}) X_{i_{ref},EC} \\ \frac{\partial X_{ref,EC}}{\partial Q^i} = \sum_{i_{ref}}^{n_{ref}} \frac{\partial f_{i_{ref}}(\mathbf{Q})}{\partial Q^i} X_{i_{ref},EC} \end{array} \right. , \quad (17)$$

the first two eigenvectors of  $A_2$  such that the squared norm gives the smallest value. More precisely, four Eckart rotation matrices have to be calculated with the following eigenvector signs: (i) the ones from the Dymarsky and Kudin procedure, (ii)  $[\mathbf{Vec}_2(1), -\mathbf{Vec}_2(2)]$ , (iii)  $[-\mathbf{Vec}_2(1), \mathbf{Vec}_2(2)]$ , and (iv)  $[-\mathbf{Vec}_2(1), -\mathbf{Vec}_2(2)]$ . Since  $\mathbf{Vec}_2(3)$  is obtained from a cross product, its sign is just the product of the  $\mathbf{Vec}_2(1)$  and  $\mathbf{Vec}_2(2)$  signs. This new procedure, although more expensive, works very well even when a large grid is used. The red curve in Fig. 3 shows the plot of  $\text{Norm}^2$  obtained with our new procedure for the 1D-model of HONO.  $\text{Norm}^2$  is now continuous over the whole range of torsional angles. Thus, our approach leads to reliable values of  $\text{Norm}^2$  for all possible values of  $\varphi_3$ . Of course, the result is the same as for the Dymarsky and Kudin procedure for small deviations from the reference geometry.

### III. MULTIREFERENCE ECKART GEOMETRIES

As mentioned in the Introduction, only a key small modification is necessary to allow for the use of Eckart conditions based on several different reference geometries. A similar procedure has probably been used by Wang and Carrington in their study of methane using Eckart conditions (see the end of Section IV of Ref. 12). In some respects, it is related to the Sayvetz approach<sup>36</sup> and the treatment of Hougen, Bunker, and Johns,<sup>45</sup> in which the Eckart conditions follow some large amplitude motion. The Eckart conditions can be used with curvilinear coordinates—for instance, Fábri *et al.*<sup>40</sup> use a so-called “flexible Eckart-embedding” along the torsional angle in the  $\text{H}_5^+$  cation—or directly within the Reaction Path Hamiltonian (RPH) method.<sup>46,47</sup>

In our approach, different reference geometries are taken into account by the use of a moving Eckart reference geometry. Then, in Eq. (14), we need to take into account the variation of the reference geometry as a function of the internal coordinates,  $\mathbf{Q}$ ,

where we have used  $n_{ref}$  reference geometries,  $X_{i_{ref},EC}$ . The  $f_{i_{ref}}(\mathbf{Q})$  are the switching functions and each of them has to give a value close to unity around its corresponding reference geometry (with the index  $i_{ref}$ ) and zero elsewhere. To avoid unphysical reference geometries, the sum of the  $f_{i_{ref}}(\mathbf{Q})$  must be close to one. Furthermore, one has to calculate the derivatives of the functions,  $\frac{\partial f_{i_{ref}}(\mathbf{Q})}{\partial Q^i}$ .

Several options are open to define the switching functions.

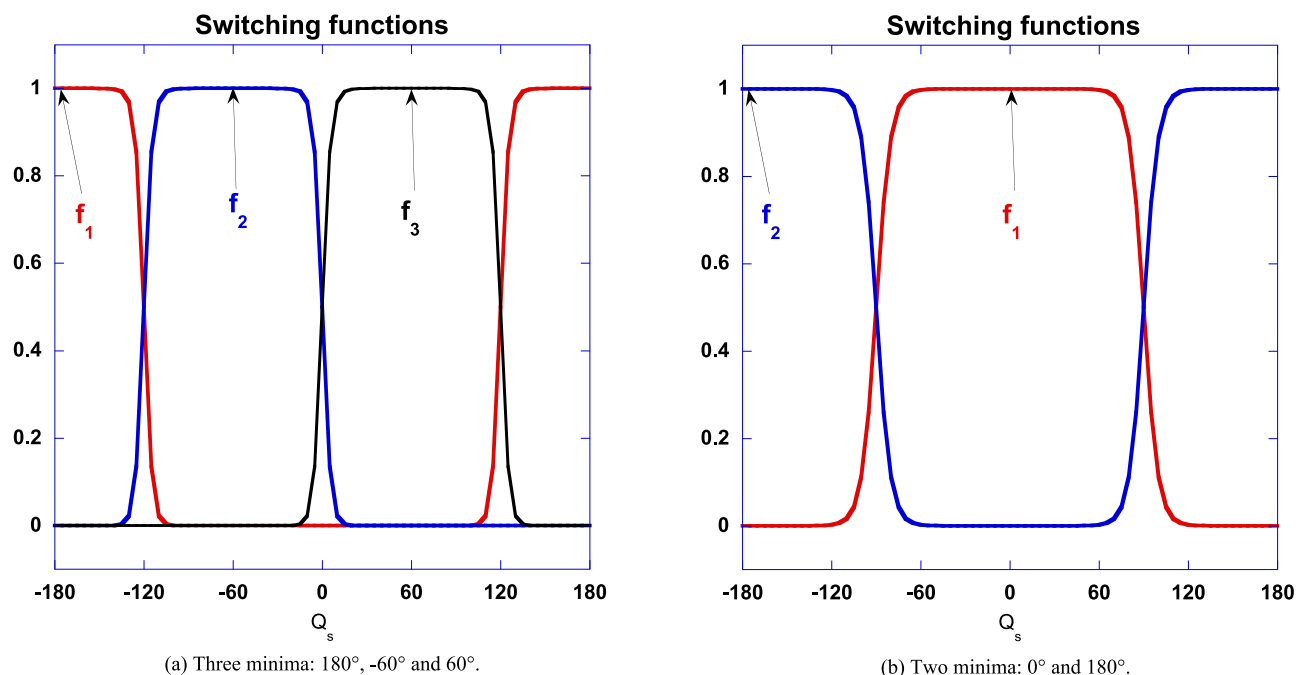


FIG. 4. Examples of switching functions  $Switch(x) = \frac{1}{2}(1 + \tanh(a \cdot x))$  along a periodic coordinate with a switching parameter  $a = 6$  for (a) a system with three minima and (b) a system with two minima. Eq. (18) has been used to define  $x$ .

- (i) The simplest option is when just one coordinate (or a few),  $Q_s$ , is substantially modified between reference geometries. For instance, if a molecular system has  $n_{ref}$  symmetric reference geometries along a periodic coordinate (dihedral angle), the switching function can be defined as

$$\left\{ \begin{array}{l} f_{i_{ref}}(Q_s) = Switch \left[ \frac{\cos(Q_s - Q_s^{i_{ref}}) - \cos\left(\frac{\pi}{n_{ref}}\right)}{1 - \cos\left(\frac{\pi}{n_{ref}}\right)} \right] \\ Q_s^{i_{ref}} = Q_s^{1_{ref}} + \frac{(i_{ref} - 1) 2\pi}{n_{ref}} \\ Switch(x) = \frac{1}{2}(1 + \tanh(a \cdot x)) \end{array} \right. \quad (18)$$

Here  $Switch(x)$  is a sigmoid function, which approaches a step function at increasingly high values of  $a$ . In the examples shown in Fig. 4, we used  $a = 6$  in the tanh function. The following figure shows the switching functions of Eq. (18) for two cases. The first is a system with three minima ( $Q_s^1 = \pi$  and the others at  $\pm\pi/3$ ) and the second is a system with two minima ( $Q_s^1 = 0$  and the other at  $\pi$ ). One can see that each curve has a flat maximum around its corresponding reference geometry (defined by the dihedral angle  $Q_s^1$ ).

- (ii) A second, more general, option is independent of the specific coordinates chosen. Here, the switching functions (see Eq. (19)) are defined using the sum of the squared differences ( $Norm^2_{i_{ref}}(\mathbf{Q})$ ) between the Cartesian coordinates of the reference geometry ( $i_{ref}$ ) and those of the deformed geometry in a given frame. This frame can be either the original non-Eckart frame,  $F$ , or the Eckart frame. In the latter case, it means we need to, first, apply the  $n_{ref}$  Eckart conditions. Then the multi-reference

switching functions are defined as

$$\left\{ \begin{array}{l} f_{i_{ref}}(\mathbf{Q}) = \frac{Exp[-a \cdot Norm^2_{i_{ref}}(\mathbf{Q})]}{\sum_{j_{ref}=1}^{n_{ref}} Exp[-a \cdot Norm^2_{j_{ref}}(\mathbf{Q})]} \\ Norm^2_{i_{ref}}(\mathbf{Q}) = \sum_{\lambda=1}^N \left\| \vec{X}_{i_{ref}, EC}^\lambda - \vec{X}_{NF}^\lambda(\mathbf{Q}) \right\|^2 \end{array} \right. \quad (19)$$

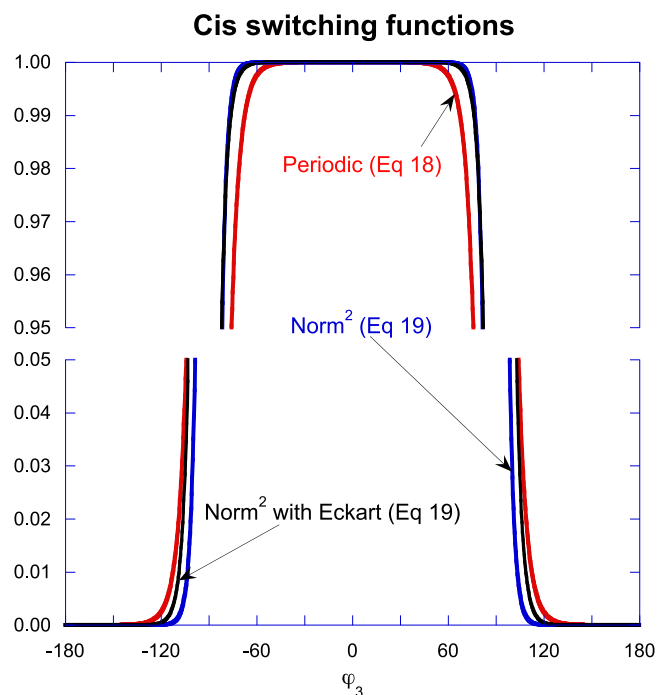


FIG. 5. Examples of switching functions for the *cis*-isomer of HONO with the parameter  $a = 6$  for all curves. See text for details.

$\vec{X}_{NF}^{\lambda}(\mathbf{Q})$  can be either  $\vec{X}_F^{\lambda}(\mathbf{Q})$  or  $\vec{X}_{EC}^{\lambda}(\mathbf{Q})$ . Also in this case, each  $f_{i_{ref}}(\mathbf{Q})$  function approaches a step function at increasingly high values of  $a$ . Using this definition, the switching functions always exactly sum up to one. We also need to calculate the derivatives of these functions. Since the derivatives of  $\vec{X}_{NF}^{\lambda}(\mathbf{Q})$  are known, we can calculate those of  $\text{Norm}_{i_{ref}}^2(\mathbf{Q})$  and then the derivatives of  $f_{i_{ref}}(\mathbf{Q})$ .

The three switching functions along the torsional angle,  $\varphi_3$  for the *cis* isomer of HONO (see Fig. 2): (i) Eq. (18), (ii) Eq. (19) with the non-Eckart frame, and (iii) Eq. (19) with the Eckart frame are shown in Fig. 5. It can be seen that all three are almost identical. It is important to stress that the calculations of the switching functions using Eq. (19) need only the Cartesian coordinates, although we have plotted them as a function of the torsional angle.

#### IV. APPLICATIONS

In the present study, the HONO molecule is employed to check our implementation of the Eckart conditions with several reference geometries, using the PES and dipole moments obtained by Richter *et al.*<sup>41,42</sup> The computational details are presented in Section IV A. In Section IV B, the  $J = 1$  and  $J = 5$  rotational levels are calculated for both the *cis* and *trans* isomers. Finally, the vibrational intensities are computed in Section IV C.

##### A. Computational details

In order to minimize the computational resources needed to calculate the (ro)-vibrational levels, we have carried out a sequence of coordinate transformations (schematized in Fig. 6) to describe both isomers in a well-balanced way: (i) *z-matrix transformation*. This first transformation defines the six internal coordinates,  $\mathbf{Q}^{\text{zmat}}$  ( $r_1, r_2, \theta_2, r_3, \theta_3$ , and  $\varphi_3$ ) from a set of Cartesian coordinates,  $\mathbf{Q}^{\text{cart}}$ . (ii) *Flexible transformation*. Except for  $\varphi_3$ , the five remaining internal coordinates are shifted to their optimal values along the torsional path,  $\mathbf{Q}^{\text{zmat,opt}}$  (obtained from the minimization of the Richter PES), to form the flexible coordinates,  $\mathbf{Q}_k^{\text{flex}}$  with  $k = 1 \dots 5$ . (iii) *Normal coordinates transformation*,  $\mathbf{Q}^{\text{NM}}$ . To reduce the quadratic couplings, the five flexible coordinates are transformed to get physically well-adapted curvilinear normal coordinates.<sup>48–50</sup> However, the Hessian and the kinetic contributions for these five coordinates are averaged over both the *trans* and the *cis* isomers.<sup>51</sup> (iv) *Active transformation*,

$\mathbf{Q}^{\text{act}}$ . When full dimensionality is used, this transformation is the identity,  $\mathbf{Q}^{\text{act}} = \mathbf{Q}^{\text{NM}}$ . In general, however, it can be used to set up constraints or reduced dimensionality models, which separate the active coordinates from the inactive ones. In the present study, this feature is used to define a 1D-contracted basis set associated with the torsion as an active coordinate.

In a way, our coordinates are similar to those used in a RPH,<sup>46</sup> in particular the RPH implemented in the program Multimode<sup>47</sup> or related approaches developed by Meyer and Günthard<sup>52</sup> and Hougen *et al.*<sup>45</sup> The main difference concerns the curvilinear normal modes, which are unique in our case (based on averaged Hessian and kinetic contributions), while theirs follow the isomerization path.

The vibrational multidimensional basis set used in our calculations was defined as follows:

- (i) A 5D-harmonic oscillator (HO) basis set was used for all five curvilinear normal coordinates ( $Q_k$ ,  $k = 1 \dots 5$ ) along the torsional path. These basis functions were selected in terms of excitation level,  $L_B$ . More precisely, we kept a basis function,  $\prod_{k=1}^5 HO_{i_k}(Q_k)$ , ( $HO =$  Harmonic oscillator) when the sum of the  $i_k$  is smaller or equal to  $L_B$ .<sup>51,53</sup> With this basis set, a Smolyak sparse grid<sup>54,51,53,55,56</sup> can be used with a Smolyak parameter,  $L_{smol}$ , which determines the size of the grid.<sup>51</sup>
- (ii) A 1D-basis set in the torsional coordinate containing 20 contracted basis functions was obtained from a Fourier series with 64 sine or cosine functions and 80 grid points. The contracted basis functions are the eigenstates of a 1D-flexible model Hamiltonian along the torsional path (see Refs. 51 and 53) and are obtained automatically in ELVIBROT.<sup>57</sup>

Next, to calculate the vibrational intensities or the rotational levels, we have used two different approaches to get the vibrational wave functions ( $J = 0$ ).

- (i) For the vibrational intensities:

The 5D-basis set has 3003 basis functions and 109 207 grid points (with  $L_B = 10$  and  $L_{smol} = 11$ ).<sup>51</sup> Thus, the 6D basis has 60 060 ( $3003 \times 20$ ) basis functions. The eigenstates up to  $4000 \text{ cm}^{-1}$  above the vibrational zero point energy were then obtained through an iterative block-Davidson procedure, described in Ribeiro *et al.*<sup>58</sup> that does not involve storing the Hamiltonian matrix. Fundamental transition frequencies were converged to within  $0.1 \text{ cm}^{-1}$  and the wave functions were analyzed

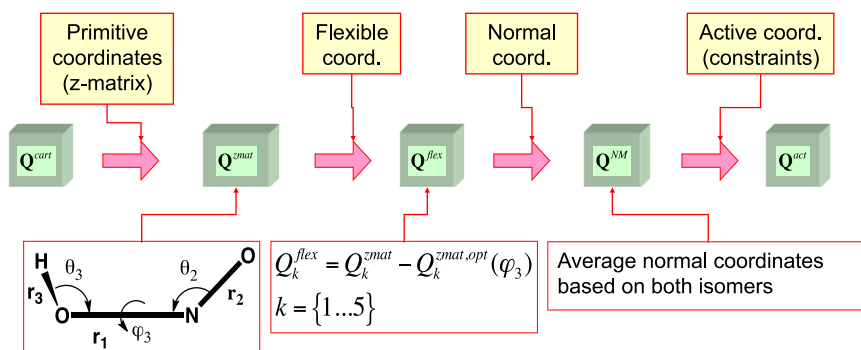


FIG. 6. Scheme describing the coordinate transformations. The coordinates on the right are the active ones,  $\mathbf{Q}^{\text{act}}$ , used during the dynamics, while the coordinates on the left are the Cartesian ones,  $\mathbf{Q}^{\text{cart}}$ , required in TNUM.

using the 1D-reduced density associated with each 1D-basis set. This procedure enabled us to automatically label each level in terms of the dominant 1D-basis function. The dominant basis function associated with the torsion ( $\varphi_3$ ) allowed us to label each level as *cis* or *trans*. Indeed, the 1D-torsional basis is obtained through a contraction procedure and the first 13 basis functions are strictly localized around each isomer.

(ii) For the rotational levels:

To converge the rotational levels in a rovibrational expansion, the vibrational basis set size needs to be smaller than the one used for the vibrational intensities. For this purpose, we used a 5D-basis set with 252 basis functions and 6788 grid points ( $L_B = 5$  and  $L_{smol} = 7$ ). Thus, the 6D basis has only 5040 ( $252 \times 20$ ) basis functions, which allowed us to perform a standard diagonalization of the Hamiltonian matrix.

The subsequent calculation of rovibrational levels is rather standard; we followed the approach used by Yurchenko *et al.*<sup>11</sup> and Csaba *et al.*<sup>44</sup> For a given value of the total angular momenta,  $J$ , the usual  $|J, K, M\rangle$  basis functions were utilized, where  $K$  and  $M$  are the quantum numbers associated to the  $z$ -components of the molecular frame (Eckart or not) and the space-fixed frame, respectively. Since  $M$  is a good quantum number, only  $2J + 1$  basis functions with  $K \in [-J, \dots, J]$  are needed.

The  $\hat{J}_x$ ,  $\hat{J}_y$ , and  $\hat{J}_z$  operators projected in the non-Eckart frame or the Eckart frame are represented in the  $|J, K, M\rangle$  basis as complex matrices for which the only non-zero element is the following.<sup>44,59</sup>

$$\begin{cases} \langle J, K, M | \hat{J}_z | J, K, M \rangle = \hbar^2 K \\ \langle J, K, M | \hat{J}_x | J, K \pm 1, M \rangle = \frac{1}{2} \hbar^2 \sqrt{J(J+1) - K(K \pm 1)} \\ \langle J, K, M | \hat{J}_y | J, K \pm 1, M \rangle = \mp \frac{i}{2} \hbar^2 \sqrt{J(J+1) - K(K \pm 1)} \end{cases} \quad (20)$$

These relations are obtained using the anomalous commutations relations, since the  $\hat{J}_x$ ,  $\hat{J}_y$ , and  $\hat{J}_z$  operators are projected in the molecular frame (non-Eckart or Eckart).<sup>59</sup> Next, these matrices are transformed to the Wang basis,  $|W_{JKM}^\pm\rangle$ ,<sup>11,12,44,59</sup> which enables to express the  $\hat{J}_x$ ,  $\hat{J}_y$ , and  $\hat{J}_z$  operators as purely imaginary matrices,  $\mathbf{J}_W^x$ ,  $\mathbf{J}_W^y$ , and  $\mathbf{J}_W^z$ ,

$$\begin{cases} |W_{J0M}^+\rangle = |J, 0, M\rangle & \text{for } K = 0 \\ |W_{JKM}^+\rangle = \frac{1}{\sqrt{2}} (|J, K, M\rangle + |J, -K, M\rangle) & \text{for } K \text{ even} \\ |W_{JKM}^-\rangle = \frac{1}{\sqrt{2}} (|J, K, M\rangle - |J, -K, M\rangle) & \text{for } K \text{ odd} \\ |W_{JKM}^-\rangle = \frac{i}{\sqrt{2}} (|J, K, M\rangle - |J, -K, M\rangle) & \text{for } K \text{ even} \\ |W_{JKM}^-\rangle = \frac{i}{\sqrt{2}} (|J, K, M\rangle + |J, -K, M\rangle) & \text{for } K \text{ odd} \end{cases} \quad (21)$$

The others operators,  $\hat{J}_\alpha^2$  and  $(\hat{J}_\alpha \hat{J}_\beta + \hat{J}_\beta \hat{J}_\alpha)$ , present in the rovibrational Hamiltonian (Eq. (5) and (6)) are projected on the Wang basis,  $\mathbf{J}_W^{\alpha\alpha}$  and  $\mathbf{J}_W^{\alpha\beta}$ , using sums and products of the

$\mathbf{J}_W^\alpha$  matrices. Finally, the rovibrational Hamiltonian matrix,  $\mathbf{H}_{RV}$ , which is real, is built up as follows:

$$\mathbf{H}_{RV} = \mathbf{I}_w \otimes \mathbf{H}_{def} + \sum_\alpha \mathbf{J}_W^\alpha \otimes \mathbf{T}_{cor}^\alpha + \sum_{\alpha \geq \beta} \mathbf{J}_W^{\alpha\beta} \otimes \mathbf{T}_{rot}^{\alpha\beta}, \quad (22)$$

where  $\mathbf{I}_w$  is the identity matrix in the Wang basis and  $\mathbf{H}_{def}$ ,  $\mathbf{T}_{cor}^\alpha$ , and  $\mathbf{T}_{rot}^{\alpha\beta}$  are, respectively, the matrix representation of the  $\hat{\mathbf{H}}_{def}$  ( $\hat{\mathbf{T}}_{def} + \mathbf{V}$ ),  $\hat{\mathbf{T}}_{cor}^\alpha$ , and  $\hat{\mathbf{T}}_{rot}^{\alpha\beta}$  (see Eqs. (4)-(6)) in a vibrational basis, which will be specified below.

## B. Rotational levels

As mentioned in the introduction, one of us has calculated the rovibrational levels of the *trans* HONO isomer and H<sub>2</sub>O using the TNUM implementation with the single-reference Eckart conditions and the MCTDH method.<sup>13</sup> In that paper, the rovibrational levels were obtained using the Eckart and non-Eckart frames with almost identical results in both cases, thereby showing the correctness of the Eckart implementation in TNUM. Here, however, we have added a new feature in the Eckart implementation: *the Eckart reference geometry can be switched from one reference geometry (cis isomer) to another one (trans isomer)*. Therefore, we performed several rotational calculations (in a rovibrational basis expansion) where the vibrational basis is made up of eigenfunctions,  $|\Psi_p^V\rangle$ , at  $J = 0$  (2 or 1000 functions for different calculations). This vibrational basis enables us to easily analyze the  $l$ th rovibrational states,  $|\Psi_I^{RV}\rangle$ , with the help of the population on the  $p$ th vibrational level,<sup>13,60,61</sup>  $\rho_I^p$ ,

$$\begin{aligned} |\Psi_I^{RV}\rangle &= \sum_{p=1}^{nb\_Vib} \sum_{r=1}^{2J+1} C_I^{pr} |W_r\rangle |\Psi_p^V\rangle, \\ \rho_I^p &= \sum_{r=1}^{2J+1} |\langle W_r \cdot \Psi_p^V | \Psi_I^{RV} \rangle|^2 = \sum_{r=1}^{2J+1} |C_I^{pr}|^2, \end{aligned} \quad (23)$$

where  $|W_r\rangle$  is one of the rotational Wang basis functions given in the following order:  $[|W_{J0M}^+\rangle, \dots, |W_{JJM}^+\rangle, |W_{J1M}^-\rangle, \dots, |W_{JJM}^-\rangle]$ .

The rotational energy levels associated with the vibrational ground state of both HONO isomers calculated using ELVIBROT are presented for  $J = 1$  in Table I and for  $J = 5$  in Table II. We note first of all that the comparison between the converged rotational energies (Eckart with multireference geometry, column 3) and the ones obtained with MCTDH<sup>13,60</sup> (column 2) shows excellent agreement, since the largest difference is only about  $0.03 \text{ cm}^{-1}$  (Table II).

When the vibrational basis is large enough, the rotational energy levels should be identical for all molecular frames. For  $J = 1$ , the largest energy difference between the converged rotational energies (column 3, Eckart with multireference) and the rotational energies using non-Eckart frame (column 4) is about  $0.002 \text{ cm}^{-1}$  for both isomers, while this energy difference increases to  $0.2 \text{ cm}^{-1}$  for  $J = 5$ . This larger difference is due to an insufficient number of vibrational levels ( $nb\_Vib = 1000$ ). Indeed, when rotational calculations are performed with 500 vibrational states, the largest energy differences increase,  $0.03 \text{ cm}^{-1}$  for  $J = 1$  and  $0.6 \text{ cm}^{-1}$  for  $J = 5$ .

Furthermore, as expected, for the calculations at  $J > 0$ , the vibrational population of the rotational levels demonstrates

TABLE I.  $J = 1$  rotational energies (in  $\text{cm}^{-1}$ ) from MCTDH (Ref. 60 for the *cis* isomer) and from calculations with and without Eckart conditions (single reference or multireference). Numbers in parentheses: population,  $\rho_I^P$ , of the main vibrational state,  $|\Psi_P^V\rangle$ .

Label	MCTDH	Eckart with multireference	Without Eckart	Eckart with <i>trans</i> -reference	Eckart with <i>cis</i> -reference	Eckart with multireference
		nb_Vib = 1000	nb_Vib = 1000	nb_Vib = 2	nb_Vib = 2	nb_Vib = 2
<i>Trans</i> isomer	/	<b>0.782</b>	0.783 (0.99)	<b>0.783</b>	0.817	<b>0.783</b>
		<b>3.450</b>	3.451 (0.98)	<b>3.457</b>	5.619	<b>3.457</b>
		<b>3.500</b>	3.501 (0.97)	<b>3.507</b>	5.646	<b>3.507</b>
<i>Cis</i> isomer	0.81	<b>0.815</b>	0.815 (0.99)	0.851	<b>0.815</b>	<b>0.815</b>
	3.17	<b>3.170</b>	3.172 (0.98)	5.156	<b>3.176</b>	<b>3.176</b>
	3.23	<b>3.230</b>	3.232 (0.97)	5.193	<b>3.236</b>	<b>3.236</b>

the efficient separation between the rotational and vibrational contributions.<sup>13,61</sup> Indeed, when the correct Eckart conditions are used, only one vibrational state is populated (population greater than 0.99; not shown in table). In particular, this is true in the case when the rotational levels of a given isomer are calculated with the corresponding Eckart reference geometry (not shown in the table) as well as when the rotational levels are calculated for both isomers using the Eckart multireference geometry approach. However, when the Eckart conditions are not used (or used with the wrong reference geometry), the vibrational populations of the main vibrational state become smaller than one (see the numbers in parentheses in column 4 of Tables I and II). In particular for  $J = 5$ , the lowest population drops to 0.54 for the *trans* isomer of the 10th and 11th rotational states associated with the ground vibrational state.

The excellent separation between the vibrational and rotational motions at  $J > 0$  when the Eckart conditions are

used, yields almost converged rotational energy levels for both isomers with only two vibrational levels ( $\text{nb\_Vib} = 2$ , one for the *trans* isomer and the other one for the *cis* isomer). Indeed, the largest energy difference between the converged rotational energies (third column, with  $\text{nb\_Vib} = 1000$ ) and the rotational energies using Eckart conditions with the *trans* isomer (fifth column) or with *cis* isomer (sixth column) is smaller than  $0.01 \text{ cm}^{-1}$  at  $J = 1$  (Table I, bold values of columns 5 and 6) and about  $0.2 \text{ cm}^{-1}$  at  $J = 5$  (Table II, bold values of columns 5 and 6). Of course, here we have to consider only the energy levels of a given isomer with its corresponding Eckart reference geometry. One could note also that the rotational states calculated without Eckart frame and with  $\text{nb\_Vib} = 2$  (not shown in the tables) are very different from the converged rotational levels. In particular for  $J = 1$  and for the *trans* isomer, the rotational energy levels are 2.12, 21.37, and  $21.42 \text{ cm}^{-1}$  which are several time larger than the converged ones.

TABLE II.  $J = 5$  rotational energies (in  $\text{cm}^{-1}$ ) from MCTDH (Ref. 13 for *trans* and Ref. 60 for *cis* isomer) and calculated with and without Eckart conditions (single reference or multireference). Numbers in parentheses: population,  $\rho_I^P$ , of the main vibrational state,  $|\Psi_P^V\rangle$ .

Label	MCTDH	Eckart with multireference	Without Eckart	Eckart with <i>trans</i> -reference	Eckart with <i>cis</i> -reference	Eckart with multireference	
		nb_Vib = 1000	nb_Vib = 1000	nb_Vib = 2	nb_Vib = 2	nb_Vib = 2	
<i>Trans</i> isomer	11.71	<b>11.71</b>	11.73 (0.88)	<b>11.71</b>	12.25	<b>11.72</b>	
	14.05	<b>14.05</b>	14.07 (0.91)	<b>14.06</b>	16.86	<b>14.06</b>	
	14.80	<b>14.80</b>	14.82 (0.81)	<b>14.81</b>	17.27	<b>14.81</b>	
	22.50	<b>22.50</b>	22.53 (0.82)	<b>22.53</b>	31.51	<b>22.54</b>	
	22.53	<b>22.53</b>	22.56 (0.82)	<b>22.56</b>	31.52	<b>22.56</b>	
	35.97	<b>35.96</b>	36.01 (0.76)	<b>36.03</b>	55.60	<b>36.04</b>	
	35.97	<b>35.96</b>	36.01 (0.76)	<b>36.03</b>	55.60	<b>36.04</b>	
	54.80	<b>54.79</b>	54.87 (0.66)	<b>54.93</b>	89.31	<b>54.93</b>	
	54.80	<b>54.79</b>	54.87 (0.66)	<b>54.93</b>	89.31	<b>54.93</b>	
	79.01	<b>78.98</b>	79.09 (0.54)	<b>79.22</b>	132.65	<b>79.21</b>	
	79.01	<b>78.98</b>	79.09 (0.54)	<b>79.22</b>	132.65	<b>79.21</b>	
	<i>Cis</i> isomer	12.18	<b>12.18</b>	12.21 (0.88)	12.76	<b>12.19</b>	<b>12.19</b>
		14.15	<b>14.15</b>	14.18 (0.92)	16.81	<b>14.16</b>	<b>14.17</b>
15.05		<b>15.05</b>	15.09 (0.81)	17.37	<b>15.06</b>	<b>15.06</b>	
21.76		<b>21.76</b>	21.81 (0.83)	30.06	<b>21.77</b>	<b>21.79</b>	
21.80		<b>21.80</b>	21.86 (0.83)	30.07	<b>21.83</b>	<b>21.83</b>	
33.70		<b>33.69</b>	33.77 (0.78)	51.68	<b>33.75</b>	<b>33.76</b>	
33.70		<b>33.69</b>	33.78 (0.78)	51.68	<b>33.75</b>	<b>33.76</b>	
50.39		<b>50.38</b>	50.52 (0.70)	81.94	<b>50.49</b>	<b>50.49</b>	
50.39		<b>50.38</b>	50.52 (0.70)	81.94	<b>50.49</b>	<b>50.49</b>	
71.84		<b>71.82</b>	72.01 (0.60)	120.85	<b>72.01</b>	<b>72.01</b>	
71.84	<b>71.82</b>	72.01 (0.60)	120.85	<b>72.01</b>	<b>72.01</b>		

TABLE III. Fundamental vibrational transition frequencies (in  $\text{cm}^{-1}$ ) and intensities ( $\text{km mol}^{-1}$ ) for the *trans*-isomer of HONO at 1 K calculated with and without Eckart conditions. The Eckart calculations are done separately with a *trans*-isomer reference and with a *cis*-isomer reference.

Label	Fundamental transitions ( $\text{cm}^{-1}$ )	Intensities ( $\text{km mol}^{-1}$ )		
		Without Eckart	Eckart with <i>trans</i> -isomer reference	Eckart with <i>cis</i> -isomer reference
Torsion	537.7	100.5	76.2	170.2
ONO bend	600.9	135.5	113.6	112.0
NO stretch	795.8	130.9	148.7	152.3
HON bend	1267.6	171.9	189.0	178.5
N=O stretch	1689.7	161.7	142.3	143.9
OH stretch	3590.2	59.3	58.1	54.6

Finally, the use of a multireference geometry (using the switch function  $\text{Norm}^2$ ; Eq. (19)) with the Eckart conditions gives almost the same results as when the Eckart conditions are applied with a single *trans*-reference geometry (last column of Tables I and II). The differences, all of them smaller than  $0.02 \text{ cm}^{-1}$ , are due to the use of a small value of the scaling parameter which gives smoother switching functions than the ones shown in Fig. 5. Therefore, the molecular frame with multireference geometries is slightly different than the usual Eckart frame.

For the  $J > 0$  calculations using the Eckart multireference approach, the value of the switching parameter,  $a$  (Eqs. (18) and (19)), has to be well chosen to avoid numerical problems. Indeed, when  $a$  is too large, the switching function becomes a step-like function and the numerical integration becomes less precise. Therefore, the rovibrational Hamiltonian becomes non-Hermitian unless a large grid is used. In the present calculations, the value  $a = 6$  was too large with the number of grid points (80) used along the torsion, so we have chosen the value  $a = 2$ , which enabled us to perform the calculations without trouble.

### C. Vibrational intensities

The transition intensity,  $I(f \leftarrow i)$ , between an initial level,  $i$ , and a final level,  $f$ , may be calculated

using the standard formula (see chapter 14.1 of Ref. 21),

$$I(f \leftarrow i) \propto (E_f - E_i)(\text{pop}_i - \text{pop}_f) \langle \Psi_i^V | \vec{\mu} | \Psi_f^V \rangle^2, \quad (24)$$

where  $E_p$ ,  $\text{pop}_p$ , and  $\Psi_p^V$  are, respectively, the energy, the Boltzmann population, and the vibrational wave function of the level  $p$  ( $p = i$  or  $f$ ). Although we discuss only fundamental transitions, the previous expression (Eq. (24)) is general and valid also for overtones and combination bands.

At low temperature (1 K), only the *trans* isomer is populated and then only the transitions of that isomer are obtained. Our results calculated without the Eckart conditions (Table III, third column) are in excellent agreement with those computed by Richter *et al.* (cf. Table V of Ref. 42). In Table III, one can also see the influence of the Eckart Frame. Indeed, except for the OH stretch, the intensities of the fundamental transitions are quite different when the Eckart conditions are used (4th vs. 3rd column). This effect is well known; see, for instance, the work of Le Sueur *et al.* on the  $\text{H}_2\text{S}$  molecule.<sup>2</sup> Furthermore, if one uses the *cis*-reference (5th column) geometry, the intensity for the torsion is different from the intensity obtained using the *trans*-reference geometry (4th column). Finally, the use of a multireference geometry with the Eckart conditions gives exactly the same results as when

TABLE IV. Fundamental transition frequencies (in  $\text{cm}^{-1}$ ) and intensities ( $\text{km mol}^{-1}$ ) for HONO at 300K calculated with and without Eckart conditions. For the calculations with Eckart conditions, the multireference results are compared with those obtained using a single reference at either the *trans* or *cis* geometry (columns in bold).

Label	Transitions ( $\text{cm}^{-1}$ )	Intensities ( $\text{km mol}^{-1}$ )			
		Without Eckart	Eckart with <i>trans</i> -reference	Eckart with <i>cis</i> -reference	Eckart with multireference
<i>Trans</i> isomer	Torsion	48.9	<b>37.1</b>	82.9	<b>37.1</b>
	ONO bend	67.4	<b>56.5</b>	55.7	<b>56.5</b>
	NO stretch	67.5	<b>76.6</b>	78.5	<b>76.6</b>
	HON bend	90.4	<b>99.3</b>	93.8	<b>99.3</b>
	N=O stretch	85.2	<b>74.9</b>	75.8	<b>74.9</b>
	OH stretch	31.3	<b>30.7</b>	28.8	<b>30.7</b>
<i>Cis</i> isomer	ONO bend	10.8	7.2	<b>7.4</b>	<b>7.4</b>
	Torsion	31.5	38.3	<b>20.7</b>	<b>20.7</b>
	NO stretch	93.0	100.9	<b>99.6</b>	<b>99.6</b>
	HON bend	2.5	3.0	<b>2.6</b>	<b>2.6</b>
	N=O stretch	59.5	48.3	<b>47.8</b>	<b>47.8</b>
	OH stretch	5.7	5.7	<b>6.1</b>	<b>6.1</b>

the Eckart conditions are applied with a single *trans*-reference geometry. For this application, we could use  $a = 6$  for the switching parameter, because this value did not give rise to a non-Hermitian Hamiltonian.

The energy difference between the ground state vibrational levels of the two isomers is about  $94 \text{ cm}^{-1}$ . Therefore, at 300K, the population of the *cis*-isomer is 39.0% of the total and transitions from both isomers are visible.<sup>43</sup> In Table IV, the vibrational intensities are reported at 300K. In this case, the advantage of employing the Eckart conditions with multi-reference geometries is that the frequencies and intensities of the infrared spectra of both isomers are obtained with only one calculation. With a single reference, two calculations would be required. In the fourth and fifth columns of Table IV, we have reported the vibrational intensities calculated using Eckart conditions with a single reference geometry. In the fourth column, the *trans*-minimum is used as Eckart reference geometry and only the *trans*-transitions have correct vibrational intensities (bold values), while in the fifth column, the *cis*-minimum is used and the correct intensities correspond only to the *cis*-transitions (bold values). The vibrational transitions obtained (column 6) with a multireference geometry (with the *trans*-minimum and *cis*-minimum reference geometries) are identical (within  $0.01 \text{ km mol}^{-1}$ ) with those obtained with a single reference geometry. Furthermore, for this comparison, the three definitions of the switching functions have been used and they give the same results.

It is also interesting to note that satisfying the Eckart conditions is necessary for a good rotation-vibration separation but not sufficient since, of course, the choice of the “correct” reference geometry is also required. So, the results in column 5 (noted “Eckart with *trans*-reference”) for the *cis*-isomer and in column 6 (Eckart with *cis*-reference) for the *trans*-isomer reflect a poor rotation-vibration separation because, although the Eckart conditions are fulfilled, the “wrong” reference geometry is used.

## V. CONCLUSIONS

Although numerical implementations of the Eckart conditions have been available for many years, in this study, we propose a new numerical and exact procedure, which completely avoids a finite difference scheme to get the kinetic energy operator for curvilinear coordinates. The Watson Hamiltonian<sup>9</sup> and the geometrical approach of Pesonen<sup>34</sup> also avoid finite differences, but only for specific coordinates, namely, normal and polyspherical coordinates. Recently, Szalay<sup>35</sup> has proposed an interesting two-step strategy in which the Watson Hamiltonian is transformed from the normal coordinates to another set of coordinates without resorting to finite differences. On the other hand, our implementation is completely general and can be used with all sets of coordinates already present in TNUM. In particular, the primitive internal coordinates could be defined using a z-matrix or polyspherical coordinates (with Jacobi, Radau, valence vectors, and also with sub-systems).<sup>62,63</sup> In addition, we can add transformations (linear combinations, flexible transformations, normal modes,

and many others) to adapt the coordinates for the process under study.<sup>51</sup>

The program TNUM is highly modular. Therefore, it is easy to modify the procedure to calculate the Eckart rotation matrix. Here, we have adapted the Dymarsky and Kudin procedure,<sup>18</sup> but other approaches could be tested, like the recent one proposed by Krasnoshchekov *et al.*<sup>19</sup> In particular, it would be interesting if this new approach enabled one to avoid the Norm<sup>2</sup> test (Eq. (2)) on the four Eckart rotation matrices to prevent axis switching (see Fig. 3).

Our new implementation enables us to use Eckart conditions for molecular systems with a moving reference geometry. Of course, this approach is related to the Sayvetz conditions,<sup>36</sup> which can be viewed as an extension of the Eckart conditions for molecular systems with one or several large amplitude motions. In the Sayvetz approach, the rotational Eckart conditions are applied with a moving reference geometry,  $X_{ref,EC}(\mathbf{Q})$ , along the coordinates,  $Q_s$ , associated with the large amplitude motions (the first Sayvetz condition; see below). The  $X_{ref,EC}(\mathbf{Q})$  are usually the Cartesian coordinates of the optimal geometry,  $X_{opt,EC}(Q_s)$ , along one or several  $Q_s$ . In other words, the Eckart reference geometry changes continuously along a chemical or physical path in  $Q_s$ . In our approach, the moving geometry is defined using several reference geometries and switching functions so that knowledge of a chemical or physical path is not required.

Another condition is added in the Sayvetz approach to reduce the coupling between the coordinates,  $Q_s$ , associated with the large amplitude motions (see also Eq. (4.9) of Ref. 64),

$$\sum_{\lambda=1}^N m_{\lambda} \cdot \sum_{\alpha=x,y,z} (X_{EC}^{\lambda,\alpha}(\mathbf{Q}) - X_{ref,EC}^{\lambda,\alpha}(\mathbf{Q})) \frac{\partial X_{ref,EC}^{\lambda,\alpha}(\mathbf{Q})}{\partial Q_s} = 0. \quad (25)$$

In our approach, we do not impose this Sayvetz condition because it is almost fulfilled around the reference geometries. Indeed, when the current geometry is close to one of the reference geometries (among the  $n_{ref}$  ones), the values of the switching functions are almost constant (see Fig. 5), and therefore, the derivatives of the moving reference geometry with respect to any coordinates are zero ( $\frac{\partial X_{ref,EC}^{\lambda,\alpha}(\mathbf{Q})}{\partial Q_s} = 0$ ). Furthermore, when the current geometry is in between two or more reference geometries, the derivatives in Eq. (25) are not zero anymore, but the value of the wave function is zero when the energy barriers between the minima are high. Therefore, for a high barrier case, the effect of Eq. (25) does not really matter.

Of course, when the system is really floppy with low barriers between minima, the Sayvetz conditions are required. We could easily modify our implementation to use the moving reference geometry along a path like the Sayvetz one as in the approach used by Fábri *et al.*<sup>40</sup> In that case, the second Sayvetz relation (Eq. (25)) could be fulfilled, for instance, by using Szalay’s approach.<sup>65</sup>

Our approach can be applied to molecular systems with several minima separated with a large barrier,<sup>66,67</sup> like  $\text{NH}_3$



$$\left\{ \begin{array}{l} \theta = \frac{1}{2} \tan^{-1} \left( \frac{M_{pq}^{(j)}}{\delta} \right) \quad \text{for } |M_{pq}^{(j)}| \leq |\delta| \\ \theta = \frac{1}{2} \tan^{-1} \left( \frac{\delta}{M_{pq}^{(j)}} \right) - \frac{\pi}{2} \quad \text{for } |M_{pq}^{(j)}| > |\delta| \text{ and } M_{pq}^{(j)} > 0 \\ \theta = \frac{1}{2} \tan^{-1} \left( \frac{\delta}{M_{pq}^{(j)}} \right) + \frac{\pi}{2} \quad \text{for } |M_{pq}^{(j)}| > |\delta| \text{ and } M_{pq}^{(j)} \leq 0 \end{array} \right. \quad (\text{B3})$$

Here,  $\delta = \frac{M_{pp}^{(j)} - M_{qq}^{(j)}}{2}$ ; the comparison between  $|M_{pq}^{(j)}|$  and  $|\delta|$  avoids small denominators.

- <sup>1</sup>C. Eckart, *Phys. Rev.* **47**, 552 (1935).  
<sup>2</sup>C. R. Le Sueur, S. Miller, J. Tennyson, and B. T. Sutcliffe, *Mol. Phys.* **76**, 1147 (1992).  
<sup>3</sup>A. Urru, I. N. Kozin, G. Mulas, B. J. Braams, and J. Tennyson, *Mol. Phys.* **108**, 1973 (2010).  
<sup>4</sup>S. N. Yurchenko, R. J. Barber, A. Yachmenev, W. Thiel, P. Jensen, and J. Tennyson, *J. Phys. Chem. A* **113**, 11845 (2009).  
<sup>5</sup>J. M. Luis, M. Duran, J. L. Andrés, B. Champagne, and B. Kirtman, *J. Chem. Phys.* **111**, 875 (1999).  
<sup>6</sup>S. Carter, J. M. Bowman, and N. C. Handy, *Theor. Chem. Acc.* **100**, 191 (1998).  
<sup>7</sup>P. Cassam-Chenaï and J. Liévin, *J. Chem. Phys.* **136**, 174309 (2012).  
<sup>8</sup>M. Rey, A. V. Nikitin, and V. G. Tyuterev, *J. Quant. Spectrosc. Radiat. Transfer* **164**, 207 (2015).  
<sup>9</sup>J. K. G. Watson, *Mol. Phys.* **15**, 479 (1968).  
<sup>10</sup>E. Mátyus, G. Czakó, B. T. Sutcliffe, and A. G. Császár, *J. Chem. Phys.* **127**, 084102 (2007).  
<sup>11</sup>S. N. Yurchenko, W. Thiel, and P. Jensen, *J. Mol. Spectrosc.* **245**, 126 (2007).  
<sup>12</sup>X.-G. Wang and T. Carrington, *J. Chem. Phys.* **138**, 104106 (2013).  
<sup>13</sup>K. Sadri, D. Lauvergnat, F. Gatti, and H.-D. Meyer, *J. Chem. Phys.* **141**, 114101 (2014).  
<sup>14</sup>F. Jorgensen, *Int. J. Quantum Chem.* **14**, 55 (1978).  
<sup>15</sup>K. N. Kudin and A. Y. Dymarsky, *J. Chem. Phys.* **122**, 224105 (2005).  
<sup>16</sup>A. B. McCoy, D. C. Burleigh, and E. L. Sibert, *J. Chem. Phys.* **95**, 7449 (1991).  
<sup>17</sup>C. Fábri, E. Mátyus, and A. G. Császár, *Spectrochim. Acta, Part A* **119**, 84 (2014).  
<sup>18</sup>A. Y. Dymarsky and K. N. Kudin, *J. Chem. Phys.* **122**, 124103 (2005).  
<sup>19</sup>S. V. Krasnoshchekov, E. V. Isayeva, and N. F. Stepanov, *J. Chem. Phys.* **140**, 154104 (2014).  
<sup>20</sup>S. R. Polo, *J. Chem. Phys.* **24**, 1133 (1956).  
<sup>21</sup>P. R. Bunker and P. Jensen, *Molecular Symmetry and Spectroscopy* (NRC Research, Ottawa, 1998).  
<sup>22</sup>H. Wei and T. J. Carrington, *J. Chem. Phys.* **107**, 2813 (1997).  
<sup>23</sup>H. Wei and T. J. Carrington, *J. Chem. Phys.* **107**, 9493 (1997).  
<sup>24</sup>H. Wei, *J. Chem. Phys.* **118**, 7208 (2003).  
<sup>25</sup>H. Wei, *J. Chem. Phys.* **118**, 7202 (2003).  
<sup>26</sup>X. Chapuisat, A. Nauts, and J.-P. Brunet, *Mol. Phys.* **72**, 1 (1991).  
<sup>27</sup>D. Lauvergnat and A. Nauts, *J. Chem. Phys.* **116**, 8560 (2002).  
<sup>28</sup>E. Mátyus, G. Czakó, and A. Császár, *J. Chem. Phys.* **130**, 28 (2009).  
<sup>29</sup>M. Harthcock and J. Laane, *J. Mol. Spectrosc.* **324**, 300 (1982).  
<sup>30</sup>M. Senent, *Chem. Phys. Lett.* **296**, 299 (1998).  
<sup>31</sup>A. Niño and C. Muñoz-Caro, *Comput. Chem.* **18**, 27 (1994).  
<sup>32</sup>D. Strobusch and C. Scheurer, *J. Chem. Phys.* **135**, 144101 (2011).  
<sup>33</sup>T. Szidarovszky, C. Fábri, and A. G. Császár, *J. Chem. Phys.* **136**, 174112 (2012).  
<sup>34</sup>J. Pesonen, *J. Chem. Phys.* **140**, 074101 (2014).  
<sup>35</sup>V. Szalay, *J. Chem. Phys.* **142**, 174107 (2015).  
<sup>36</sup>A. Sayvetz, *J. Chem. Phys.* **7**, 383 (1939).  
<sup>37</sup>B. Kirtman, *J. Chem. Phys.* **37**, 2516 (1962).  
<sup>38</sup>B. Kirtman, *J. Chem. Phys.* **41**, 775 (1964).  
<sup>39</sup>H. Lin, W. Thiel, S. N. Yurchenko, M. Carvajal, and P. Jensen, *J. Chem. Phys.* **117**, 11265 (2002).  
<sup>40</sup>C. Fábri, J. Sarka, and A. G. Császár, *J. Chem. Phys.* **140**, 051101 (2014).  
<sup>41</sup>F. Richter, M. Hochlaf, P. Rosmus, F. Gatti, and H.-D. Meyer, *J. Chem. Phys.* **120**, 1306 (2004).  
<sup>42</sup>F. Richter, F. Gatti, C. Léonard, F. Le Quéré, and H.-D. Meyer, *J. Chem. Phys.* **127**, 164315 (2007).  
<sup>43</sup>C. Deeley and I. Mills, *J. Mol. Struct.* **100**, 199 (1983).  
<sup>44</sup>C. Fábri, E. Mátyus, and A. G. Császár, *J. Chem. Phys.* **134**, 074105 (2011).  
<sup>45</sup>J. Hougen, P. Bunker, and J. Johns, *J. Mol. Spectrosc.* **34**, 136 (1970).  
<sup>46</sup>W. Miller, N. Handy, and J. Adams, *J. Chem. Phys.* **72**, 99 (1980).  
<sup>47</sup>S. Carter and N. Handy, *J. Chem. Phys.* **113**, 987 (2000).  
<sup>48</sup>E. B. Wilson, J. C. Decius, and P. C. Cross, *Molecular Vibrations: The Theory of Infrared and Raman Vibrational Spectra* (McGraw-Hill, New York, 1955).  
<sup>49</sup>C. Leforestier, A. Viel, F. Gatti, C. Muñoz, and C. Iung, *J. Chem. Phys.* **114**, 2099 (2001).  
<sup>50</sup>Y. F. Zhang, S. J. Klippenstein, and R. A. Marcus, *J. Chem. Phys.* **94**, 7319 (1991).  
<sup>51</sup>D. Lauvergnat and A. Nauts, *Spectrochim. Acta, Part A* **119**, 18 (2014).  
<sup>52</sup>R. Meyer and H. H. Günthard, *J. Chem. Phys.* **50**, 353 (1969).  
<sup>53</sup>D. Lauvergnat and A. Nauts, *Phys. Chem. Chem. Phys.* **12**, 8405 (2010).  
<sup>54</sup>G. Avila and T. Carrington, *J. Chem. Phys.* **131**, 174103 (2009).  
<sup>55</sup>S. A. Smolyak, *Sov. Math. Dokl.* **4**, 240 (1963).  
<sup>56</sup>G. Avila and T. Carrington, *J. Chem. Phys.* **135**, 064101 (2011).  
<sup>57</sup>D. Lauvergnat, EIVibRot: Quantum Dynamics code, available at <http://pagesperso.lcp.u-psud.fr/lauvergnat/EIVibRot/EIVibRot.html>.  
<sup>58</sup>F. Ribeiro, C. Iung, and C. Leforestier, *J. Chem. Phys.* **123**, 054106 (2005).  
<sup>59</sup>R. N. Zare, *Angular Momentum: Understanding Spatial Aspects in Chemistry and Physics* (Wiley-Interscience, New York, 1988).  
<sup>60</sup>M. Sala, F. Gatti, D. Lauvergnat, and H.-D. Meyer, *Phys. Chem. Chem. Phys.* **14**, 3791 (2012).  
<sup>61</sup>E. Mátyus, C. Fábri, T. Szidarovszky, G. Czakó, W. D. Allen, and A. G. Császár, *J. Chem. Phys.* **133**, 034113 (2010).  
<sup>62</sup>F. Gatti and C. Iung, *Phys. Rep.* **484**, 1 (2009).  
<sup>63</sup>M. Ndong, L. Joubert-Doriol, H.-D. Meyer, A. Nauts, F. Gatti, and D. Lauvergnat, *J. Chem. Phys.* **136**, 034107 (2012).  
<sup>64</sup>G. O. Sørensen, *Top. Curr. Chem.* **82**, 97 (1979).  
<sup>65</sup>V. Szalay, *J. Chem. Phys.* **140**, 234107 (2014).  
<sup>66</sup>J. M. Luis, H. Reis, M. Papadopoulos, and B. Kirtman, *J. Chem. Phys.* **131**, 034116 (2009).  
<sup>67</sup>M. Garcia-Borràs, M. Solà, D. Lauvergnat, H. Reis, J. M. Luis, and B. Kirtman, *J. Chem. Theory Comput.* **9**, 520 (2013).